ChemComm

COMMUNICATION

View Article Online
View Journal | View Issue

Cite this: *Chem. Commun.*, 2021, 57, 6566

Received 19th May 2021,
Accepted 4th June 2021

DOI: 10.1039/d1cc02624k

rsc.li/chemcomm

The number and shape of lattice solvent molecules controls spin-crossover in an isomorphous series of crystalline solvate salts†‡

Izar Capel Berdiell,[ab] Rafal Kulmaczewski,[a] Namrah Shahid, [a] Oscar Cespedes[c] and Malcolm A. Halcrow *[a]

Crystals of [FeL_2][BF_4]$_2$·*n*MeCN (*L* = *N*-(2,6-di{pyrazol-1-yl}pyrid-4-yl)acetamide; *n* = 1 or 2) and [FeL_2][ClO_4]$_2$·MeCN are isomorphous. When *n* = 1 the compounds exhibit an abrupt, hysteretic spin-transition below 200 K, but when *n* = 2 the material remains high-spin on cooling. [FeL_2]X_2·EtCN (X^- = BF_4^- or ClO_4^-) are isomorphous with the MeCN solvates and undergo their spin-transition at almost the same temperature. However this now occurs in two-steps *via* a re-entrant mixed-spin intermediate phase, which correlates with crystallographic ordering of the bent propionitrile molecule.

Crystal engineering of spin-crossover (SCO) molecular materials is of continuing interest, for their development as molecular switches for macro-, micro- and nanoscale device applications.[1] Such compounds also have wider relevance, as models for mechanistic studies of phase transitions in molecular crystals.[2] Isomorphous families of compounds are particularly useful in that regard, in showing how small structure changes can influence the temperature and cooperativity of a thermal spin transition within the same crystal lattice structure.[3] While some groups of isomorphous compounds exhibit very consistent SCO behaviour,[4–6] in other cases a surprising variation in the cooperativity or occurrence of SCO is observed.[7–11]

We recently described the solvate crystals [FeL_2]X_2·Me_2CO (**1**X_2·Me_2CO, Scheme 1; *L* = *N*-(2,6-di{pyrazol-1-yl}pyrid-4-yl)acetamide; X^- = BF_4^- or ClO_4^-). The BF_4^- salt undergoes an abrupt spin-transition on cooling which proceeds to *ca.* 50% completeness, and is accompanied by an unusual crystallographic symmetry breaking involving a twelve-fold expansion of the unit cell.[12] We were therefore keen to investigate other solvate crystals of these complex salts. We now present the acetonitrile and propionitrile solvates of **1[BF$_4$]$_2$** and **1[ClO$_4$]$_2$**, a family of isomorphous materials where the influence of lattice solvent on their spin state properties is especially clearly defined.

Slow crystallisation of **1[BF$_4$]$_2$** from MeCN/Et_2O yielded two different phases, **1[BF$_4$]$_2$**·*n*MeCN (*n* = 1 and 2). The pseudopolymorphs adopt the same space group (triclinic, $P\bar{1}$, Z = 2) with similar unit cell dimensions, but have different spin-state properties. **1[BF$_4$]$_2$**·MeCN undergoes an abrupt and hysteretic spin-transition at $T_{1/2}\downarrow$ = 185 ± 5 K and $T_{1/2}\uparrow$ = 195 ± 5 K from a variable temperature unit cell study (Fig. S7, ESI‡). In contrast, **1[BF$_4$]$_2$**·2MeCN remains high-spin at 120 K. Analogous recrystallisations of **1[ClO$_4$]$_2$** gave the SCO-active phase **1[ClO$_4$]$_2$**·MeCN as the only isolable product, which showed $T_{1/2}\downarrow$ = 155 ± 5 K and $T_{1/2}\uparrow$ = 165 ± 5 K (Fig. S9, ESI‡). Both mono-acetonitrile solvates undergo their hysteretic SCO without a crystallographic phase change.

The molecular geometries in **1[BF$_4$]$_2$**·2MeCN, **1[BF$_4$]$_2$**·MeCN and **1[ClO$_4$]$_2$**·MeCN are very similar (Table S2, ESI‡). The high-spin molecules have a twisted coordination geometry with *trans*-*N*{pyridyl}–Fe–*N*{pyridyl} angles (ϕ) of 166.04(7)–168.66(14)°. Published high-spin salts of $[Fe(bpp)_2]^{2+}$ (bpp = 2,6-di{pyrazol-1-yl}-pyridine) derivatives show a range of ϕ values between

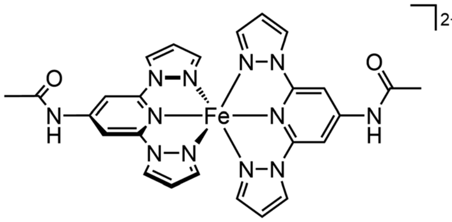

Scheme 1 The structure of **1**X_2·solv (X^- = BF_4^- or ClO_4^-; solv = MeCN, EtCN, $MeNO_2$, MeOH or EtOH).

[a] School of Chemistry, University of Leeds, Woodhouse Lane, Leeds LS2 9JT, UK. E-mail: m.a.halcrow@leeds.ac.uk
[b] Institute of Electronic Structure and Laser, Foundation for Research and Technology–Hellas, P.O. Box 1527, Heraklion GR-711 10, Greece
[c] School of Physics and Astronomy, University of Leeds, EC Stoner Building, Leeds LS2 9JT, UK

† Data associated with this study are available from the University of Leeds library at http://doi.org/10.5518/999.

‡ Electronic supplementary information (ESI) available: Experimental procedures and characterisation data; crystallographic figures and tables; X-ray powder diffraction, TGA and DSC analyses; and additional solid and solution phase magnetic data. CCDC 2078647–2078664. For ESI and crystallographic data in CIF or other electronic format see DOI: 10.1039/d1cc02624k

$150 \leq \phi \leq 180°$, and are less likely to exhibit SCO as ϕ decreases.[13,14] That reflects the unfavourable activation barrier required to transform a highly distorted high-spin molecule in a solid lattice, to the more regular coordination geometry ($\phi > 170°$) preferred by the low-spin state.[13,15] The $\phi = 167 \pm 1°$ distortion in high-spin **1X₂**·nMeCN lies on the cusp, where SCO is possible but is rarely observed in practise.[16] However, when high-spin $[Fe(bpp)_2]^{2+}$ salts with that degree of distortion do undergo SCO, the large structural rearrangement involved imparts cooperativity to the transition.[16,17] Thus, the change in ϕ between the spin states is $\Delta\phi = 5.9(2)°$ in **1[BF$_4$]$_2$**·MeCN and 6.6(2)° in **1[ClO$_4$]$_2$**·MeCN, which leads to atomic displacements of up to 1.0 Å at the periphery of the molecules during SCO (Fig. S4, ESI‡). This structural rearrangement is the most likely source of the abrupt, hysteretic cooperativity in their spin-transitions.

The cations and anions in **1X$_2$**·*n*MeCN form discrete $[\{FeL_2\}X_2]$ assemblies by N–H···F or N–H···O hydrogen bonding. The cations associate into chains by translation along the crystallographic *a* direction, through weak intermolecular π···π overlap of their pyrazolyl rings. The only other close inter-cation contact is a C–H···H–C steric clash involving another pyrazolyl group, in molecules related by the crystallographic inversion centre. That contact only occurs in the high-spin crystals with $n = 1$, and leads to disorder of that pyrazolyl ring. The basic disposition of the cations, anions and solvent in **1[BF$_4$]$_2$**·MeCN is reproduced in **1[BF$_4$]$_2$**·2MeCN (Fig. 1).

The extra solvent molecules in **1[BF$_4$]$_2$**·2MeCN form centrosymmetric pairs within a new cavity centred at lattice coordinates 1/2, 1/2, 0 (Fig. 1, top). This cavity has a volume of 145 Å^3, and is created by the following changes in **1[BF$_4$]$_2$**·2MeCN compared to **1[BF$_4$]$_2$**·MeCN: a *ca.* 1.5 Å displacement of nearest neighbour cations within the (100) plane, which also changes the handedness of the triclinic unit cell from $\alpha < 90°$ to $\alpha > 90°$;[18] a *ca.* 5° rotation of the cation within its lattice site, which is coupled to a small decrease in ϕ; and 0.5–0.8 Å displacements of each anion. Notably the extensive anion and solvent disorder in high-spin **1[BF$_4$]$_2$**·MeCN is mostly quenched in **1[BF$_4$]$_2$**·2MeCN. That implies the packing in the latter crystal is generally more compact.

Freshly prepared **1[BF$_4$]$_2$**·*n*MeCN is predominantly the $n = 2$ phase by microanalysis and TGA (Fig. S11 and S12, ESI‡). The material loses 1 equiv. MeCN abruptly at 368 K in the TGA, with the second equivalent being lost more gradually on further heating; the solvent-free material is only achieved above *ca.* 500 K. Samples of **1[BF$_4$]$_2$**·*n*MeCN lose one equivalent of MeCN on drying *in vacuo* at room temperature, affording analytically pure **1[BF$_4$]$_2$**·MeCN (Fig. 2). In contrast, only the SCO-active phase **1[ClO$_4$]$_2$**·MeCN is apparent in that compound by powder diffraction and TGA. Both **1X$_2$**·MeCN materials retain 1 equiv. MeCN upon drying *in vacuo* at room temperature.

Magnetic susceptibility data from these phases agree well with their crystal structures. Thus **1[BF$_4$]$_2$**·2MeCN remains high-spin between 5–300 K, while **1[BF$_4$]$_2$**·MeCN and **1[ClO$_4$]$_2$**·MeCN exhibit abrupt, hysteretic spin-transitions at $T_{1/2}$ = 189 and 165 K respectively (Table 1). Samples of **1[BF$_4$]$_2$**·*n*MeCN transform to the pure **1[BF$_4$]$_2$**·MeCN phase inside the vacuum of the magnetometer cavity, unless the sample is protected against solvent loss during measurement (Fig. 2). Magnetic data from **1[ClO$_4$]$_2$**·MeCN also contain a small fraction of a

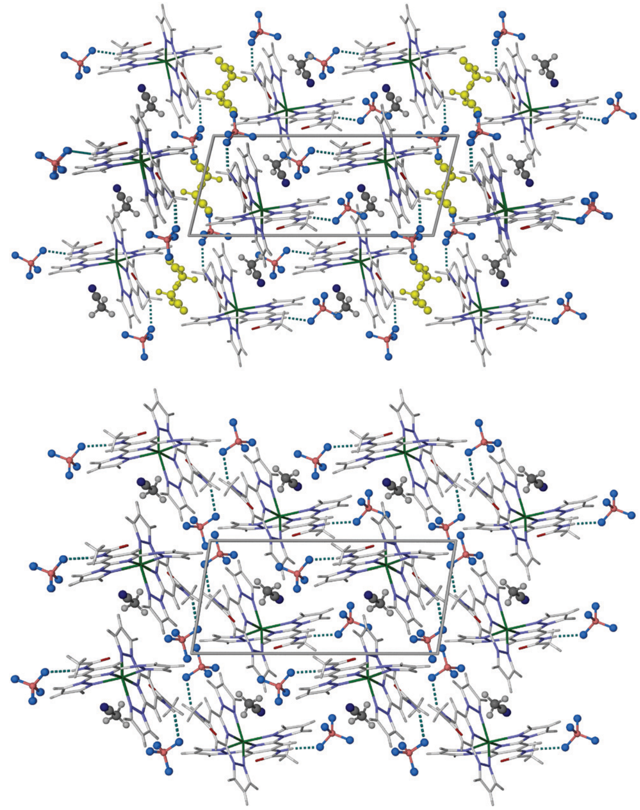

Fig. 1 Packing diagrams of **1[BF$_4$]$_2$**·2MeCN (top) and the high-spin form of **1[BF$_4$]$_2$**·MeCN (bottom), viewed parallel to the [010] vector with *c* horizontal. Only one orientation of disordered residues is included, and the cations are de-emphasised for clarity. The extra solvent molecules in **1[BF$_4$]$_2$**·2MeCN are highlighted in yellow.

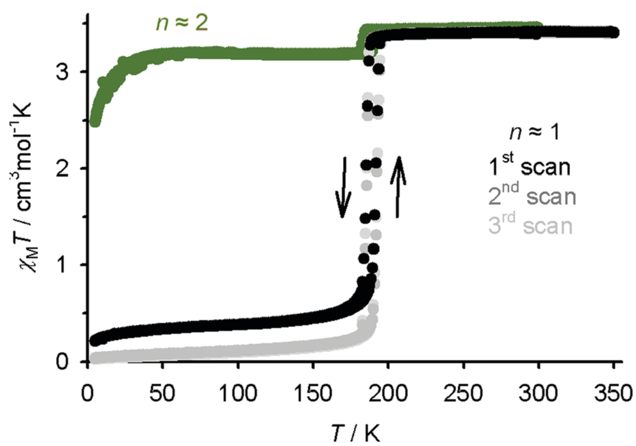

Fig. 2 Magnetic data for **1[BF$_4$]$_2$**·*n*MeCN, measured in cooling and warming modes at scan rate 5 K min^{-1}. The sample for the green data was protected from *in situ* solvent loss (ESI‡), and is mostly **1[BF$_4$]$_2$**·2MeCN with <10% of the $n = 1$ phase. The black and grey data were measured without special precautions, causing partial desolvation of the sample inside the magnetometer. The first scan shows a *ca.* 9 : 1 ratio of **1[BF$_4$]$_2$**·MeCN and **1[BF$_4$]$_2$**·2MeCN, which transforms to pure **1[BF$_4$]$_2$**·MeCN in the second and third scans after heating to 350 K.

high-spin phase, although this appears to be solvent-free material generated by *in situ* solvent loss (Fig. S13, ESI‡).

The propionitrile solvates **1X₂**·EtCN (X^- = BF_4^- or ClO_4^-) are isomorphous with the acetonitrile crystals (triclinic, $P\bar{1}$, Z = 2). They are phase-pure by powder diffraction, and are also highly stable to solvent loss by TGA (Fig. S26 and S27, ESI‡). These also exhibit abrupt and hysteretic thermal spin-transitions, but now with a clear plateau near 50% conversion (Fig. 3). Interestingly, the average $T_{1/2}$ for the two SCO steps in each $\mathbf{1X_2}$·EtCN material corresponds well with $T_{1/2}$ for the one-step SCO in the corresponding $\mathbf{1X_2}$·MeCN sample (Table 1).

The discontinuous SCO in $\mathbf{1[ClO_4]_2}$·EtCN reflects re-entrant crystallographic symmetry-breaking to an intermediate phase (phase 2) near the midpoint temperature of the spin-transition (Fig. S22, ESI‡).[19,20] The intermediate phase (triclinic, $P\bar{1}$, Z = 4) retains the same space group as the initial phase, but with a doubled unit cell volume containing 1 : 1 mixture of high- and low-spin molecules. These are segregated into alternating layers within the crystallographic (010) plane (Fig. 4).

The cation molecular structures in phases 1 and 2 resemble those in $\mathbf{1X_2}$·MeCN (Table S6, ESI‡). As well as the spin state changes, the phase transformations on cooling $\mathbf{1[ClO_4]_2}$·EtCN involve the quenching of disorder in the solvent and ClO_4^- ions. Most striking is the EtCN molecule, which is equally disordered over ''up'' and ''down'' orientations in high-spin (HS) phase 1 (Fig. S17, ESI‡). This disorder is mostly quenched in phase 2 where both unique solvent sites adopt the up configuration, but one molecule retains *ca.* 15% of the down orientation. In low-spin (LS) phase 1, the single EtCN molecule is now fully ordered in the ''up'' orientation. Hence, the phase 1(HS) → 2 → 1(LS) transformations are accompanied by stepwise crystallographic ordering of the solvent molecules in the lattice.

No crystallographic evidence for phase 2 was found in $\mathbf{1[BF_4]_2}$·EtCN, whose SCO plateau spans a narrower temperature range (Fig. 3). However, that does not rule out a symmetry breaking near 190 K in that crystal, which could occur locally but without long–range order in the lattice.[20] For comparison, the mixed-anion salt $\mathbf{1[BF_4]_z[ClO_4]_{2-z}}$·EtCN ($z \approx 1$) was also crystallised. The spin-transition properties of this material lie midway between the pure BF_4^- and ClO_4^- salts, and phase 2

Table 1 Spin-crossover parameters for the isomorphous [Fe(L^1)$_2$]X$_2$·MeCN and [Fe(L^1)$_2$]X$_2$·EtCN (X^- = BF_4^- or ClO_4^-) materials from magnetic susceptibility data (Fig. 2 and 3 and ESI; scan rate 5 K min^{-1})

	$T_{1/2}\downarrow$/K	$T_{1/2}\uparrow$/K	$T_{1/2}$/K	$\Delta T_{1/2}$/K
$\mathbf{1[BF_4]_2}$·MeCN	185	192	189	7
$\mathbf{1[ClO_4]_2}$·MeCN	159	171	165	12
$\mathbf{1[BF_4]_2}$·EtCN[a]	191	192	192	1
	181	181	181	—
$\mathbf{1[ClO_4]_2}$·EtCN[a]	180	185	183	5
	145	156	151	11
$\mathbf{1[BF_4]_z[ClO_4]_{2-z}}$·EtCN[a]	188	192	190	4
	168	172	170	4

[a] This transition proceeds in two equal steps, separated by a plateau at around 50% conversion.

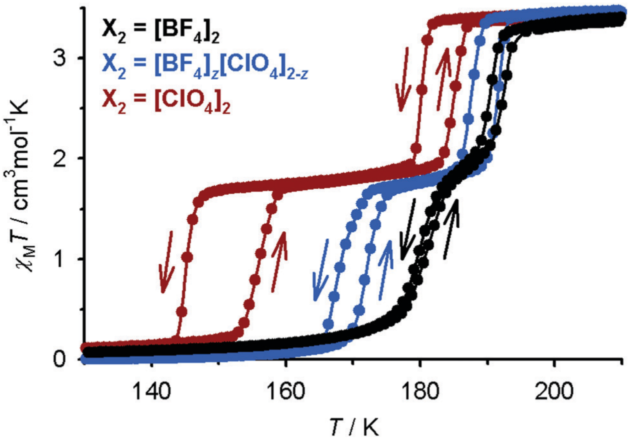

Fig. 3 Magnetic data for $\mathbf{1X_2}$·EtCN (X^- = BF_4^-, black; X^- = ClO_4^-, red; mixed-anion, blue). Data points for each compound are connected by spline curves for clarity. Data were measured in cooling and warming modes, at scan rate 5 K min^{-1}.

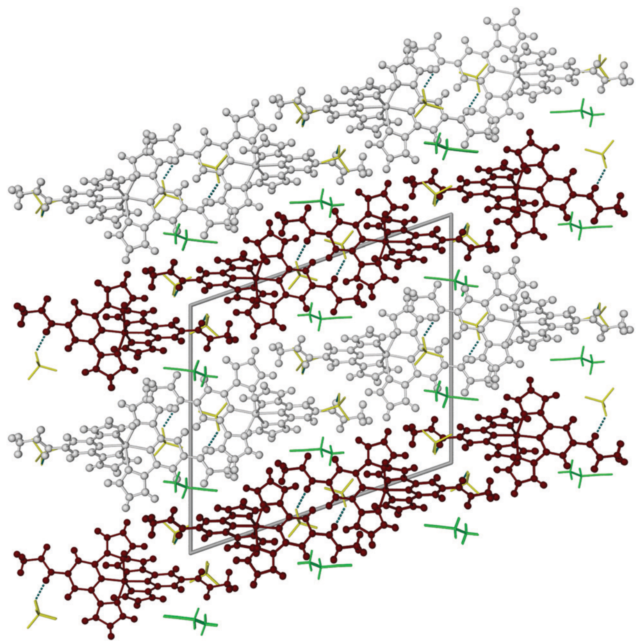

Fig. 4 Packing diagram of the mixed-spin phase 2 of $\mathbf{1[ClO_4]_2}$·EtCN, showing the segregation of high-spin (white) and low-spin (brown) cations into layers along (010). The view is along the [100] crystal vector, with the unit cell b axis vertical. The anions (yellow) and solvent molecules (green) are de-emphasised for clarity, and only the major orientation of the disordered EtCN molecule is shown.

was again observed crystallographically in its plateau temperature region. The ordering of the EtCN molecule between the phases of the mixed-anion crystal follows the same sequence as in $\mathbf{1[ClO_4]_2}$·EtCN.

Crystal structures of $\mathbf{1X_2}$·2MeNO$_2$ (X^- = BF_4^- or ClO_4^-), $\mathbf{1[BF_4]_2}$·MeOH and $\mathbf{1[ClO_4]_2}$·1/2EtOH are presented in the ESI.‡ These materials remain high-spin on cooling which, in some cases, can be related to a strong ϕ distortion in their molecular geometries, as above.[13–15] Solutions of **1[BF$_4$]$_2$** in CD_3CN and $(CD_3)_2CO$ exhibit SCO on cooling, with $T_{1/2}$ = 201 ± 2 K (Fig. S33, ESI‡). That agrees reasonably with our published correlation for pyridyl-substituted $[Fe(bpp)_2]^{2+}$ derivatives,[21] which predicts $T_{1/2}$ = 190 K for $[FeL_2]^{2+}$ bearing NHC{O}R pyridyl substituents with a σ_P^+ Hammett parameter of −0.6.[22]

This study gives new insight into the importance of lattice solvent for SCO switching in molecular materials, which was recognised in the 1980s[23] but is rarely rationalised in detail.[9–11,24] SCO in **1X$_2$**·MeCN, containing linear MeCN molecules, occurs cooperatively in one step. However, the extra solvent equivalent in **1[BF$_4$]$_2$**·2MeCN quenches the SCO, without changing its crystal symmetry or the molecular structure of the complex. That could simply reflect more compact crystal packing in the presence of the extra solvent molecule, which would inhibit the structural changes associated with SCO.[25]

The same lattice in **1X$_2$**·EtCN exhibits two-step SCO *via* a re-entrant mixed-spin intermediate phase. This correlates with a crystallographic order/disorder transition between two orientations of the bent propionitrile molecule. Discontinuous spin-transitions involving re-entrant intermediate crystal phases are well-known.[19,20] However the creation of a re-entrant mixed-spin phase during SCO in **1X$_2$**·EtCN, by simply changing the shape of the lattice solvent molecule, is a rarer observation.[9] The average $T_{1/2}$ for the two SCO steps in each EtCN solvate is the essentially same as $T_{1/2}$ for the corresponding MeCN solvate salt (Table 1). Hence, the temperature of SCO in **1X$_2$**·*n*solv (n = 1) is influenced by the X^- anion, while the solvent controls the form of the transition.

The authors thank Dr Mark Howard for the solution magnetic susceptibility measurement, and Algy Kazlauciunas for the TGA data. This work was funded by the Leverhulme Trust (RPG-2015-095) and the EPSRC (EP/K012568/1 and EP/N509681/1).

Conflicts of interest

There are no conflicts to declare.

Notes and references

1 S. Rat, M. Piedrahita-Bello, L. Salmon, G. Molnár, P. Demont and A. Bousseksou, *Adv. Mater.*, 2018, **30**, 1703862; E. Coronado, *Nat. Rev. Mater.*, 2020, **5**, 87; K. S. Kumar and M. Ruben, *Angew. Chem., Int. Ed.*, 2021, **60**, 7502.
2 M. Chergui and E. Collet, *Chem. Rev.*, 2017, **117**, 11025.
3 M. A. Halcrow, *Chem. Soc. Rev.*, 2011, **40**, 4119.
4 B. Li, R.-J. Wei, J. Tao, R.-B. Huang, L.-S. Zheng and Z. Zheng, *J. Am. Chem. Soc.*, 2010, **132**, 1558; R.-J. Wei, J. Tao, R.-B. Huang and L.-S. Zheng, *Inorg. Chem.*, 2011, **50**, 8553.
5 I. Nemec, R. Herchel and Z. Trávníček, *Dalton Trans.*, 2015, **44**, 4474.
6 M. A. Al-Azzani, F. Al-Mjeni, R. Mitsuhashi, M. Mikuriya, I. A. Al-Omari, C. C. Robertson, E. Bill and M. S. Shongwe, *Chem. – Eur. J.*, 2020, **26**, 4766.
7 P. Guionneau, J.-F. Létard, D. S. Yufit, D. Chasseau, G. Bravic, A. E. Goeta, J. A. K. Howard and O. Kahn, *J. Mater. Chem.*, 1999, **9**, 985; M. Marchivie, P. Guionneau, J.-F. Létard and D. Chasseau, *Acta Crystallogr., Sect. B: Struct. Sci.*, 2003, **59**, 479.
8 M. Yamada, H. Hagiwara, H. Torigoe, N. Matsumoto, M. Kojima, F. Dahan, J.-P. Tuchagues, N. Re and S. Iijima, *Chem. – Eur. J.*, 2006, **12**, 4536; T. Sato, K. Nishi, S. Iijima, M. Kojima and N. Matsumoto, *Inorg. Chem.*, 2009, **48**, 7211.
9 M. Hostettler, K. W. Törnroos, D. Chernyshov, B. Vangdal and H.-B. Bürgi, *Angew. Chem., Int. Ed.*, 2004, **43**, 4589.
10 L. J. Kershaw Cook, R. Kulmaczewski, O. Cespedes and M. A. Halcrow, *Chem. – Eur. J.*, 2016, **22**, 1789; R. Kulmaczewski, E. Trzop, E. Collet, S. Vela and M. A. Halcrow, *J. Mater. Chem. C*, 2020, **8**, 8420.
11 W. Phonsri, P. Harding, L. Liu, S. G. Telfer, K. S. Murray, B. Moubaraki, T. M. Ross, G. N. L. Jameson and D. J. Harding, *Chem. Sci.*, 2017, **8**, 3949; R. Díaz-Torres, W. Phonsri, K. S. Murray, L. Liu, M. Ahmed, S. M. Neville, P. Harding and D. J. Harding, *Inorg. Chem.*, 2020, **59**, 13784.
12 I. Capel Berdiell, R. Kulmaczewski, O. Cespedes and M. A. Halcrow, *Chem. – Eur. J.*, 2018, **24**, 5055.
13 J. M. Holland, J. A. McAllister, C. A. Kilner, M. Thornton-Pett, A. J. Bridgeman and M. A. Halcrow, *J. Chem. Soc., Dalton Trans.*, 2002, 548.
14 L. J. Kershaw Cook, R. Mohammed, G. Sherborne, T. D. Roberts, S. Alvarez and M. A. Halcrow, *Coord. Chem. Rev.*, 2015, **289–290**, 2.
15 S. Vela, J. J. Novoa and J. Ribas-Arino, *Phys. Chem. Chem. Phys.*, 2014, **16**, 27012.
16 L. J. Kershaw Cook, F. L. Thorp-Greenwood, T. P. Comyn, O. Cespedes, G. Chastanet and M. A. Halcrow, *Inorg. Chem.*, 2015, **54**, 6319.
17 K. S. Kumar, B. Heinrich, S. Vela, E. Moreno-Pineda, C. Bailly and M. Ruben, *Dalton Trans.*, 2019, **48**, 3825.
18 Triclinic crystals are conventionally indexed with acute or obtuse unit cell angles, depending on whether the cell displays a left- or right-handed helical canting when viewed down the shortest *a* axis (Fig. S6, ESI‡).
19 Selected examples of molecular crystals undergoing SCO *via* a re-entrant intermediate phase: D. Chernyshov, M. Hostettler, K. W. Törnroos and H.-B. Bürgi, *Angew. Chem., Int. Ed.*, 2003, **42**, 3825; V. A. Money, C. Carbonera, J. Elhaïk, M. A. Halcrow, J. A. K. Howard and J.-F. Létard, *Chem. – Eur. J.*, 2007, **13**, 5503; M. Buron-Le Cointe, N. Ould Moussa, E. Trzop, A. Moréac, G. Molnar, L. Toupet, A. Bousseksou, J. F. Létard and G. S. Matouzenko, *Phys. Rev. B: Condens. Matter Mater. Phys.*, 2010, **82**, 214106; B. J. C. Vieira, J. T. Coutinho, I. C. Santos, L. C. J. Pereira, J. C. Waerenborgh and V. da Gama, *Inorg. Chem.*, 2013, **52**, 3845; K. D. Murnaghan, C. Carbonera, L. Toupet, M. Griffin, M. M. Dîrtu, C. Desplanches, Y. Garcia, E. Collet, J. F. Létard and G. G. Morgan, *Chem. – Eur. J.*, 2014, **20**, 5613; D. J. Harding, W. Phonsri, P. Harding, K. S. Murray, B. Moubaraki and G. N. L. Jameson, *Dalton Trans.*, 2015, **44**, 15079; Z.-Y. Li, H. Ohtsu, T. Kojima, J.-W. Dai, T. Yoshida, B. K. Breedlove, W.-X. Zhang, H. Iguchi, O. Sato, M. Kawano and M. Yamashita, *Angew. Chem., Int. Ed.*, 2016, **55**, 5184; F. Fürmeyer, L. M. Carrella, V. Ksenofontov, A. Möller and E. Rentschler, *Inorg. Chem.*, 2020, **59**, 2843.
20 R. Kulmaczewski, O. Cespedes and M. A. Halcrow, *Inorg. Chem.*, 2017, **56**, 3144.
21 L. J. K. Cook, R. Kulmaczewski, R. Mohammed, S. Dudley, S. A. Barrett, M. A. Little, R. J. Deeth and M. A. Halcrow, *Angew. Chem., Int. Ed.*, 2016, **55**, 4327.
22 C. Hansch, A. Leo and R. W. Taft, *Chem. Rev.*, 1991, **91**, 165.
23 P. Gütlich, A. Hauser and H. Spiering, *Angew. Chem., Int. Ed. Engl.*, 1994, **33**, 2024.
24 See *e.g.* K. W. Törnroos, M. Hostettler, D. Chernyshov, B. Vangdal and H.-B. Bürgi, *Chem. – Eur. J.*, 2006, **12**, 6207; J. S. Costa, S. Rodríguez-Jiménez, G. A. Craig, B. Barth, C. M. Beavers, S. J. Teat and G. Aromí, *J. Am. Chem. Soc.*, 2014, **136**, 3869; D. Gentili, N. Demitri, B. Schäfer, F. Liscio, I. Bergenti, G. Ruani, M. Ruben and M. Cavallini, *J. Mater. Chem. C*, 2015, **3**, 7836.
25 There is precedent from some polymorphic SCO materials, where the lower density polymorph exhibits SCO on cooling but the higher density polymorph does not (ref. 3).